



FRIEDRICH SCHILLER UNIVERSITÄT JENA
INSTITUTE OF APPLIED PHYSICS

Efficient and High Speed Electro-Optic Modulators In Thin Film Lithium Niobate

Master Thesis

by

Efe KIRAZ

Advisor

Dr. rer. nat. Reinhard Geiß
Dr. rer. nat. habil. Frank Setzpfandt

JENA

THESIS EVALUATION FORM

We certify that we have read this thesis and that in our opinion it is fully adequate, in scope and qualify as an master of science thesis in applied physics, based on the result of the oral examination taken place on ____/____/_____

Dr. rer. nat. Reinhard Geiß
Dr. rer. nat. habil. Frank Setzpfandt
(ADVISOR)

(COMMITTEE MEMBER) (COMMITTEE MEMBER)

(CHAIRPERSON)

ABSTRACT

In this work, low-drive voltage based properties of electro-optic Mach Zehnder Modulator on thin film lithium niobate-on-insulator (LNOI) is analyzed through series of simulations in COMSOL6.0 multiphysics tool. First, the theory behind this cutting-edge modulator type is investigated with the help of well-known papers. Then $V_\pi L$ value of x-cut and z-cut LNOI is compared with previous work in literature in order to verify simulation method and physics used. Throughout simulations, optical wave and DC field distribution is analyzed and overlap integral between them is calculated by using MATLAB-COMSOL Livelink. After that, parametric sweeps was carried out to investigate how $V_\pi L$ value changes based on the geometric change. However, these changes also triggered optical losses in metallic electrode and dielectric interface. Metallic electrodes became no Sweep parameter and loss change dependence is also investigated to see outcomes of geometrical changes. Eventually, excess amount of loss in z-cut modulators was drastically affected from top silica layer thickness and advantages of x-cut modulator was observed.

Contents

ABSTRACT	I
Contents	II
List of Tables	III
List of Figures	IV
1 INTRODUCTION	1
2 THEORY	3
2.1 Maxwell's Equations	3
2.2 Transversal Field's Eigenvalue Equation	4
2.3 Electro-Optic Phenomena	5
2.3.1 Nonlinear Polarization and Index Contraction	5
2.3.2 Linear Electro-Optic Effect and Index Ellipsoid	8
2.4 Optical Waveguide	11
2.5 Coplanar Waveguide	13
2.6 Mach Zehnder Electrooptic Modulator Types	15
2.7 Electro-Optic Modulator Figure of Merits (FoM)	17
2.7.1 Half-Wave Voltage (V_π)	17
2.7.2 Modulation Bandwidth	19
2.7.3 Insertion Loss	22
2.7.4 Extinction Ratio	22
3 METHODS AND RESULTS	23
4 DISCUSSION	30
4.0.1 Future Work	31

List of Tables

1.1	Characteristic values for LiNbO ₃ at 1550nm wavelength [8]	1
1.2	Loss values for different materials [9]	2
2.1	Index contraction providing $d_{ijk} \rightarrow d_{il}$ transition	8
3.1	X-cut and Z-cut TFLN modulator dimensions and calculated $V_\pi L$ values by Zhang et al. [21]	23
3.2	Simulation results for X-cut and Z-cut Modulators	24
3.3	$V_\pi L$ voltage comparision of this work with the ones obtained by Zhang et al. [21]	24
3.4	Experimentally measured $V_\pi L$ value and its simulation results	25

List of Figures

2.1	Conceptual waveguide structure	5
2.2	Index ellipsoid method. The inner ellipse is the intersection of the index ellipsoid with the plane that is normal to \mathbf{s} and passes through the center of the ellipsoid [2]	10
2.3	Negative uniaxial crystal normal surfaces, n_o is in z-direction and n_e is in x direction [2]	10
2.4	Overlap area in ion diffused LN waveguide is more than 10 times larger with respect to monolithic-rib-ridge waveguide on the right [1].	12
2.5	Monolithic-rib-ridge waveguide consists of oxide layer and a substrate in addition to LN [1].	12
2.6	Cut direction in fabrication process determines modulator geometry [16] (the same directional reference applies also thin-film waveguides)	12
2.7	Electrodes are placed depending on crystal-cut so that overlap of fields achieved. X-cut LN is on the left and Z-cut LN is on the right	13
2.8	Generic microwave transmission line	13
2.9	Geometry of coplanar waveguide [12]	14
2.10	Unit length of coplanar waveguide	15
2.11	Phase modulator is seen on the left and MZI intensity modulator with upper and lower arms is on the right [1]	15
3.1	Optical mesh which COMSOL <i>EM Wave Frequency Domain (ewfd)</i> generates	24
3.2	DC mesh which COMSOL <i>Electrostatic (es)</i> generates	25
3.3	Transmission characteristic of sample modulator with length of 0.920cm. Red dots represents experimental data which is sampled by oscilloscope.	25
3.4	In x-cut EO MZM, top layer silica has changed and reduced	26
3.5	Plasmonic behavior in metal-LN interface. Silica layer is removed in this case.	26
3.6	In x-cut EO MZM, top layer silica (x-axis) has parametrically changed and corresponding loss values are observed.	27

3.7	In x-cut EO MZM, gap between microwave electrodes has parametrically swept.	27
3.8	In x-cut EO MZM, change of gap and its effect on optical loss is seen. Vertical scale is logarithmic.	28
3.9	In z-cut EO MZM, change of top silica layer and $V_\pi L$ value relation is seen.	28
3.10	In z-cut EO MZM, change of top silica layer has strong impact on optical loss	29
3.11	Due to severe loss, optical mode does not confine in z-cut modulator . .	29
4.1	$V_\pi L$ values are compared for different modulators.	31



1. INTRODUCTION

Electro-optic modulators are the backbone of today's data transmission systems owing to increasing data transfer rates. These building blocks make the most of relatively easy manipulation methods of electronics domain and high bandwidth, low loss data transmission capability of optical domain. In these devices, the light is modulated by radio frequency (RF), or microwave frequency, electric field and that modulation signal is generated by complementary metal-oxide-semiconductor (CMOS) electronics, which has very well defined manufacturing processes. Having a widely-adopted CMOS signal levels makes easier integration of electronic and photonic system parts.

Electro-optical modulation can be based on different phenomena for instance quadratic electro-optic effect (Kerr effect) [4], Franz–Keldysh effect [5], quantum confined stark effect [5], free-carrier plasma dispersion effect [3]. In this work, the focus of attention is on Pockels Effect due to advantages of high modulation speed and low insertion loss [5]. Pockels effect is basically change of refractive index in propotional with applied electric field in non-centrosymmetric material.

An electrooptic material is expected to have low propagation loss, agile and low-loss optical modulation, efficient optical nonlinearity. There are several options in terms of the medium where electro-optic effects take place, for instance silicone (Si) [6], indium phosphide (InP) [7], silicone nitride (SiN_x), galleium arsenide(GaAs), alimunium nitride (AlN) and silicone carbide (SiC). Nevertheless, LiNbO_3 (LN) provides these properties in a relatively diserable way such as high χ^2 nonlinearity, high Pockel's effect, high refractive index and wide transparency window [1].

Some of the important characteristic values for LiNbO_3 is seen in Table 1.1

r_{13}	r_{51}	r_{33}	r_{22}	n_o	n_e	Transparency Window
8.6 pm/V	28 pm/V	30.8 pm/V	3.4 pm/V	2.2111	2.1375	340nm - 4.6 μ m

Table 1.1: Characteristic values for LiNbO_3 at 1550nm wavelength [8]

where $r_{\#\#}$ represents the linear electro-optic tensor elements and n_o and n_e represents ordinary and extraordinary refractive indices, respectively.

In the Table 1.2, the typical loss values for several materials is seen. LN has considerably low optical insertion loss and being able to modulate refractive index of LN using RF modulation signal [9] is what makes LN indispensable, which is also the reason of using LN in this project.

Material Name	Loss (dB/cm)
InP & SiPh	>1
LN	0.1-0.01
SiN	0.01

Table 1.2: Loss values for different materials [9]

Fundamentally, this project covers the topic of linear electro-optic (EO) phenomena based Mach Zehnder Interferometer (MZI) modulator structure on thin-film LN-on-insulator (TFLNOI). It specifically focuses on simulation of $V_\pi L$ voltage at low drive levels. The reason preferring low drive voltages is that it is very first step for simulations excluding consideration of frequency dependent transmission characteristics. Also, parametric simulations are included to see $V_\pi L$ change versus the gap between coplanar waveguide electrodes and metal electrode-optical waveguide distance. These different design constraints has effect on one of the crucial parameters in MZM, the overlap integral which is basically the overlap of guided microwave field and confined optical field.

2. THEORY

This section is primarily concerned about fundamental theory which explains how linear electro-optic phenomena works. Then, theoretical equipment to analyze MZI EO modulator will be introduced. Finally, phase and amplitude modulators will be discussed.

2.1 Maxwell's Equations

Mathematical model for propagation of electromagnetic wave (EMW) in different mediums is provided by Maxwell's equations as in the following,

$$\nabla \times \mathbf{E} = -j\omega\mathbf{B} \quad (2.1a)$$

$$\nabla \times \mathbf{H} = \mathbf{J} + j\omega\mathbf{D} \quad (2.1b)$$

$$\nabla \cdot \mathbf{D} = \rho \quad (2.1c)$$

$$\nabla \cdot \mathbf{B} = 0 \quad (2.1d)$$

Here \mathbf{E} and \mathbf{H} is the electric and magnetic field vectors, respectively. \mathbf{D} and \mathbf{B} correspond to electric and magnetic flux densities. \mathbf{J} is current density and ρ is charge density, which are source of the EMW. Also, constitutive relations define relation between field vectors with their corresponding flux densities and polarization effect of the medium.

$$\mathbf{D} = \varepsilon_0\boldsymbol{\varepsilon}\mathbf{E} + \mathbf{P} \quad (2.2)$$

$$\mathbf{B} = \mu_0\mathbf{H} + \mathbf{M} \quad (2.3)$$

where ε_0 and μ_0 are vacuum dielectric permittivity and permeability, $\boldsymbol{\varepsilon}$ is relative permittivity tensor, \mathbf{P} is induced electric polarizability and \mathbf{M} is induced magnetic polarizability. Since this project does not concern with magnetic mediums, induced magnetic polarizability is basically omitted in Eq 2.3. Furthermore, this project covers materials which are homogenous and electrically anisotropic, magnetically isotropic.

2.2 Transversal Field's Eigenvalue Equation

Wave equation determines dispersion behavior in addition of electric and magnetic fields propagating in optical waveguide, they overall determine the mode characteristic. It is derived by using Eq 2.1 under charge free medium condition. Ansatz for the guided modes are,

$$\mathbf{E}(x, y, z, \omega) = \mathbf{E}(x, y, \omega)e^{-i\beta(\omega)z} \quad (2.4a)$$

$$\mathbf{H}(x, y, z, \omega) = \mathbf{H}(x, y, \omega)e^{-i\beta(\omega)z} \quad (2.4b)$$

In order to have eigenvalue equation for transverse fields, transversal and longitudinal components has to be splitted such that

$$\mathbf{E}(x, y) = \mathbf{E}_\perp + \mathbf{e}_z E_z(x, y) \quad (2.5a)$$

$$\mathbf{H}(x, y) = \mathbf{H}_\perp + \mathbf{h}_z H_z(x, y) \quad (2.5b)$$

$$\nabla = \left(\nabla_\perp, \frac{\partial}{\partial z} \right) \quad (2.5c)$$

where $\nabla_\perp = (\frac{\partial}{\partial x}, \frac{\partial}{\partial y})$. First taking the curl of 2.1a,

$$\nabla \times (\nabla \times \mathbf{E}) = -j\omega\mu_0(\nabla \times \mathbf{H}) \quad (2.6)$$

by using the vector identity $\nabla \times (\nabla \times \mathbf{E}) = \nabla(\nabla \cdot \mathbf{E}) - \nabla^2 \mathbf{E}$ Eq 2.6 becomes

$$\nabla(\nabla \cdot \mathbf{E}) - \nabla^2 \mathbf{E} = -j\omega\mu_0(\nabla \times \mathbf{H}) \quad (2.7)$$

considering charge free medium, we have $\nabla \cdot \mathbf{E} = 0$ and $\mathbf{J} = \mathbf{0}$. Also substitute Eq 2.1b into Eq 2.7 by considering Eq 2.2,

$$-\nabla^2 \mathbf{E} = -j\omega\mu_0(\nabla \times \mathbf{H}) \quad (2.8)$$

Substitute Eq 2.1b into right-hand side of Eq 2.8,

$$\nabla_\perp^2 \mathbf{E}_\perp + \frac{\omega^2}{c^2} \varepsilon(x, y) \mathbf{E}_\perp + \nabla_\perp (\mathbf{E}_\perp \nabla_\perp \ln(\varepsilon(x, y))) = \beta^2 \mathbf{E}_\perp \quad (2.9)$$

where $k(\omega)$ is wave number and defined as $\sqrt{\frac{\omega^2}{c^2} \varepsilon(\mathbf{r}, \omega)}$. Eq 2.9 is eigenvalue equation for the transversal components of the E-field in the medium which conceptually

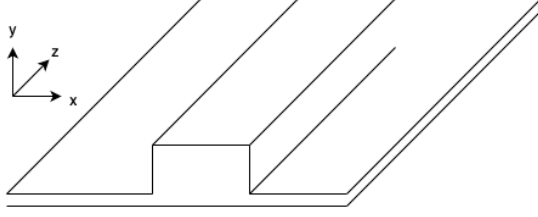


Figure 2.1: Conceptual waveguide structure

seen in Figure 2.1. In Eq 2.9 for the sake of simplicity, assumption of predominantly TE/TM polarized wave is propagating through waveguide is made and fields become independent linearly polarized. Then, Eq [2.9] becomes,

$$\nabla_{\perp}^2 \psi + \frac{\omega^2}{c^2} \epsilon(x, y) \psi - \beta^2 \psi = 0 \quad (2.10)$$

where ψ represents E_x^{op} and E_y^{op} .

2.3 Electro-Optic Phenomena

This section consists of subtopics related with nonlinear susceptibility and index contraction, linear electro-optic effect (Pockels effect), index ellipsoid and its modulation.

2.3.1 Nonlinear Polarization and Index Contraction

Polarization is expanded into its higher order nonlinear terms, which representing more precisely the contributions of higher terms such that

$$\mathbf{P} = \epsilon_0 \left[\chi^{(1)} \mathbf{E} + \chi^{(2)} \mathbf{E}^2 + \chi^{(3)} \mathbf{E}^3 \dots \right] \quad (2.11)$$

In this report, polarization is extended up to second order polarization for convenience. As a rule of thumb, susceptibility determines the relation between applied electric field and medium's response.

$$\mathbf{P}(\mathbf{r}, t) = \epsilon_0 \chi *^t \mathbf{E}(\mathbf{r}, t) \quad (2.12)$$

In Eq 2.12, symbol $*^t$ represents time convolution, which is explicitly

$$\begin{aligned} P_j(\mathbf{r}, t) = & \epsilon_0 \sum_{k=x,y,z} \int_{-\infty}^{+\infty} \chi_{ik}(\mathbf{r}, t - \tau) d\tau E_k(\mathbf{r}, \tau) + \\ & + \epsilon_0 \sum_{k=x,y,z} \sum_{l=x,y,z} \int_{-\infty}^{+\infty} \int_{-\infty}^{+\infty} \chi_{ikl}^{(2)}(\mathbf{r}, t - \tau_1, t - \tau_2) E_k(\mathbf{r}, \tau_1) E_l(\mathbf{r}, \tau_2) d\tau_1 d\tau_2 \end{aligned} \quad (2.13)$$

where $t - \tau < 0$ (or τ_1, τ_2) indicates causality of E-field and material interaction, $P_j(\mathbf{r}, t)$ subindex indicates summation of E-field contributions in three dimensions, $\chi_{jkl}^{(2)}$ represents second order nonlinear response of the medium.

In three dimensional case, \mathbf{P} and \mathbf{E} are vectors and susceptibility becomes tensor of third rank, linking one vector to the product of two others [11]. For the sake of simplicity in calculations, E-field, $\mathcal{E} \cos(\omega t - \phi)$ in time domain, is represented in frequency domain as,

$$E = E(\omega_n)e^{-i\omega t} + E^*(\omega_{-n})e^{i\omega t} \quad (2.14)$$

where $E(\omega)$ is complex amplitude and equal to $\frac{1}{2}\mathcal{E}e^{i\phi}$, where \mathcal{E} is real amplitude and ϕ is phase. It can be seen that

$$E^*(\omega) = \frac{1}{2}\mathcal{E}e^{i\phi} = E(-\omega) \quad (2.15)$$

Second order polarization term for one dimension in frequency domain is

$$P^{(2)} = \sum_{n=\pm 1} \sum_{m=\pm 2} \chi^{(2)}(\omega_n, \omega_m) E(\omega_n) E(\omega_m) e^{-i(\omega_n + \omega_m)t} \quad (2.16)$$

where susceptibility (χ) is

$$\chi^{(2)}(\omega_n, \omega_m) = -\mathcal{N}\chi^{(1)}(\omega_n)\chi^{(1)}(\omega_m)\chi^{(1)}(\omega_n + \omega_m) \quad (2.17)$$

where \mathcal{N} is a constant depending on parameters in Lorentz model with anharmonic term. Second order $\chi^{(2)}$ is multiplication of first order susceptibilities for different frequency combinations and $\chi^{(1)}$ is real when polarization frequencies are far from resonance frequency of material's constituent atoms.

As for three dimensional nonlinear polarization in frequency domain, it becomes

$$P_i^{(2)} = \sum_{jk} \sum_{nm} \chi_{ijk}^{(2)}(\omega_n + \omega_m, \omega_n, \omega_m) E_j(\omega_n) E_k(\omega_m) e^{-i(\omega_n + \omega_m)t} \quad (2.18)$$

where i,j,k each corresponds to cartesian axis x,y,z. Since $\chi^{(2)}$ is real then

$$\chi_{ijk}^{(2)}(\omega_n + \omega_m, \omega_n, \omega_m) = \chi_{ijk}^{(2)}(-\omega_n - \omega_m, -\omega_n, -\omega_m) \quad (2.19)$$

However, there are still 81 different independent nonlinear susceptibilities. According to Eq 2.17 it is possible to reduce the number of nonlinear susceptibility terms such that,

$$\chi_{ijk}^{(2)}(\omega_n + \omega_m, \omega_n, \omega_m) = \chi_{jki}^{(2)}(\omega_n, \omega_m, -\omega_n - \omega_m) = \chi_{kij}^{(2)}(\omega_m, \omega_m + \omega_n, \omega_n) \quad (2.20)$$

this means subindices i, j, k can be permuted with frequencies n, m . As a result, 81 different nonlinear susceptibilities are reduced to 27. Eq 2.18 can be written in terms of optical and electrical frequencies,

$$P_i^{(2)} = \sum_{jk} \sum_{nm} \chi_{ijk}^{(2)}(\omega_n^{opt}, \omega_m^{el}) E_j^{opt}(\omega_n^{opt}) E_k^{el}(\omega_m^{el}) e^{-i(\omega_n^{opt} + \omega_m^{el})t} \quad (2.21)$$

The frequency term $(\omega_n + \omega_m)$ in $\chi_{ijk}^{(2)}$ is dropped because optical frequency are in the range of THz and microwave frequency is in GHz range. Summation of them will approximately equal to optical frequency.

One important rule which connects nonlinear susceptibility to nonlinear electro-optic constant (d). When Eq 2.17 is generalized for three dimension,

$$\chi_{ijk}^{(2)} = \chi_{ii}^{(1)}(\omega_n) \chi_{jj}^{(1)}(\omega_m) \chi_{kk}^{(1)}(\omega_n + \omega_m) \Delta_{ijk} \quad (2.22)$$

Eq 2.22 is called as Miller rule, who found the relation and stated that Δ_{ijk} is almost constant for many materials [11]. The relation between nonlinear susceptibility or nonlinear electro-optic constant is

$$d_{ijk} = \frac{1}{2} \chi_{ijk}^{(2)} \quad (2.23)$$

Index Contraction

There is no noticeable physical correspondence to compare precedence of modulating electrical field over optical field, or vice versa. Derivations did not consider this order mathematically up to now. Here definition of column vector F indicates insignificance of multiplication order. One element of F is defined such that

$$F_l = (1 - \frac{1}{2} \delta_{jk})(E_j(\omega_{opt}) E_k(\omega_{el}) + E_k(\omega_{el}) E_j(\omega_{opt})) \quad (2.24)$$

where δ indicates Kronecker symbol and is defined as $\delta_{jk} = 1$ when $j = k$. Then \mathbf{F} is

$$\mathbf{F} = \begin{bmatrix} E_x(\omega_{opt})E_x(\omega_{el}) \\ E_y(\omega_{opt})E_y(\omega_{el}) \\ E_z(\omega_{opt})E_z(\omega_{el}) \\ E_y(\omega_{el})E_z(\omega_{opt}) + E_z(\omega_{el})E_y(\omega_{opt}) \\ E_x(\omega_{el})E_z(\omega_{opt}) + E_z(\omega_{el})E_x(\omega_{opt}) \\ E_x(\omega_{el})E_y(\omega_{opt}) + E_y(\omega_{el})E_x(\omega_{opt}) \end{bmatrix} \quad (2.25)$$

The table 2.1 shows how the index is contracted

jk	l
xx	1
yy	2
zz	3
yz/zy	4
xz/zx	5
xy/yx	6

Table 2.1: Index contraction providing $d_{ijk} \rightarrow d_{il}$ transition

Polarization and \mathbf{F} is related such that

$$P_i = 2d_{il}F_l \quad (2.26)$$

where d is defined previously in Eq 2.23. As a result, the number of elements in 2^{nd} order susceptibility tensor is reduced from 27 elements to 18 elements. Matrix form of Eq 2.26 is seen below,

$$\begin{bmatrix} P_x \\ P_y \\ P_z \end{bmatrix} = \begin{bmatrix} d_{11} & d_{12} & d_{13} & d_{14} & d_{15} & d_{16} \\ d_{21} & d_{22} & d_{23} & d_{24} & d_{25} & d_{26} \\ d_{31} & d_{32} & d_{33} & d_{34} & d_{35} & d_{36} \end{bmatrix} \begin{bmatrix} E_x(\omega_{opt})E_x(\omega_{el}) \\ E_y(\omega_{opt})E_y(\omega_{el}) \\ E_z(\omega_{opt})E_z(\omega_{el}) \\ E_y(\omega_{el})E_z(\omega_{opt}) + E_z(\omega_{el})E_y(\omega_{opt}) \\ E_x(\omega_{el})E_z(\omega_{opt}) + E_z(\omega_{el})E_x(\omega_{opt}) \\ E_x(\omega_{el})E_y(\omega_{opt}) + E_y(\omega_{el})E_x(\omega_{opt}) \end{bmatrix} \quad (2.27)$$

2.3.2 Linear Electro-Optic Effect and Index Ellipsoid

The phenomena is also known as Pockels effect, it is linear relation between applied electric field and change of refractive index. Basically, Pockels medium can alter the phase of EM wave by means of induced birefringence when polarizing electric field is applied to the medium, or Pockels cell. Here, electric field which is polarizing the medium is different than the field desired to alter its phase. This condition is critical because it makes the distinction quadratic electro-optic (Kerr-Effect) from linear electro-optic effect.

In an anisotropic medium, propagation of waves is direction dependent. This requires a wave vector \mathbf{k} definition based on propagation direction.

$$\mathbf{k} = n_s \frac{\omega}{c_0} \mathbf{s} \quad (2.28)$$

where n_s is defined as unknown refractive index which wave experience in its propagation direction which is defined by \mathbf{s} . $\frac{\omega}{c_0}$ corresponds to free space wave number for that frequency. By substituting ansatz for plane waves Eq 2.4a, 2.4b into Maxwell equations 2.1 and also considering constitutive relation Eq 2.2 and Eq 2.28, Fresnel equation is obtained to prove that different polarization of electric field \mathbf{E} experience different refractive index.

$$\frac{s_x^2}{n_s^2 - n_x^2} + \frac{s_y^2}{n_s^2 - n_y^2} + \frac{s_z^2}{n_s^2 - n_z^2} = \frac{1}{n_s^2} \quad (2.29)$$

where n_x, n_y, n_z is derived as $n_{ij} = \sqrt{\frac{\epsilon_{ij}}{\epsilon_0}}$, based on dielectric tensor ϵ

$$\epsilon = \epsilon_0 \begin{bmatrix} \epsilon_{xx} & 0 & 0 \\ 0 & \epsilon_{yy} & 0 \\ 0 & 0 & \epsilon_{zz} \end{bmatrix} = \begin{bmatrix} n_x^2 & 0 & 0 \\ 0 & n_y^2 & 0 \\ 0 & 0 & n_z^2 \end{bmatrix} = \begin{bmatrix} n_o^2 & 0 & 0 \\ 0 & n_o^2 & 0 \\ 0 & 0 & n_e^2 \end{bmatrix} \quad (2.30)$$

where n_o indicates ordinary refractive index and n_e is extraordinary refractive index. From this second order equation Eq 2.29, there will be linearly independent two linearly polarized electric flux density. They will be later used in index ellipsoid. For LN which belongs to class of negative uniaxial crystals, dielectric tensor components in each direction is related such that $\epsilon_{zz} < \epsilon_{xx} = \epsilon_{yy}$.

According to Yariv and Pochi, propagation of electromagnetic wave in linear electro-optic medium is best described in terms of index ellipsoid [2].

$$D_i = \epsilon_{ij} E_j^{el} \quad (2.31)$$

The equation 2.32 defines constant energy density in \mathbf{D} -space.

$$U_e = \frac{1}{2} \mathbf{D} \cdot \mathbf{E} = \frac{1}{2} \mathbf{D} \epsilon_0^{-1} (\epsilon^{-1} \cdot \mathbf{D}) = \frac{1}{2\epsilon_0} \left[\frac{D_x^2}{\epsilon_{xx}} + \frac{D_y^2}{\epsilon_{yy}} + \frac{D_z^2}{\epsilon_{zz}} \right] \quad (2.32)$$

where ϵ_{ii} ($i = x, y, z$) are defined in Eq 2.30.

In order to define principle indices of refraction, the relation $\mathbf{r} = \frac{\mathbf{D}}{\sqrt{2\epsilon_0 U_e}}$ is defined. Then index ellipsoid can be written such that,

$$\frac{x^2}{n_x^2} + \frac{y^2}{n_y^2} + \frac{z^2}{n_z^2} = 1 \quad (2.33)$$

Eq 2.33 is mainly used to determine electric flux density vectors and is demonstration of Fresnel equation Eq 2.29. Index ellipsoid and the plane, which is normal to the direction of propagation \mathbf{s} , intersects each other. This intersection has ellipse shape in anisotropic materials and axes of this ellipse has length of $2n_1$ and $2n_2$, indicating two orthogonal directions.

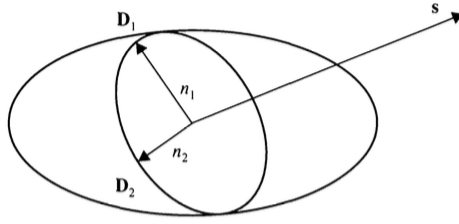


Figure 2.2: Index ellipsoid method. The inner ellipse is the intersection of the index ellipsoid with the plane that is normal to \mathbf{s} and passes through the center of the ellipsoid [2]

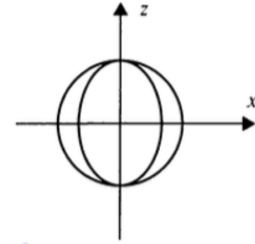


Figure 2.3: Negative uniaxial crystal normal surfaces, n_o is in z -direction and n_e is in x direction [2]

In Eq 2.33, each $\frac{1}{n_i^2}$ ($i = 1, 2, 3$) corresponds to principle values of impermeability tensor, defined as

$$\eta = \frac{\epsilon_0}{\epsilon} \quad (2.34)$$

Application of electric field causes redistribution of charges in material and slight deformation in crystal structure. Net change is the change of impermeability tensor.

$$\Delta\eta_{ij} = \eta(\mathbf{E}) - \eta(0) \equiv \Delta \left(\frac{1}{n^2} \right)_{ij} \equiv r_{ijk} E_k^{el} \quad (2.35)$$

where E_k indicates modulating electric field in x, y, z -directions and r_{ijk} corresponds to linear electro-optic coefficients. As for LN, it belongs to 3m crystal symmetry class, which leads to linear electro-optic tensor r_{ij} in the form,

$$r_{ij} = \begin{bmatrix} 0 & -r_{22} & r_{13} \\ 0 & r_{22} & r_{13} \\ 0 & 0 & r_{33} \\ 0 & r_{51} & 0 \\ r_{51} & 0 & 0 \\ -r_{22} & 0 & 0 \end{bmatrix} \quad (2.36)$$

and deformed index ellipsoid is,

$$\left(\frac{1}{n_o^2} + r_{13}E^{el}\right)x^2 + \left(\frac{1}{n_o^2} + r_{13}E^{el}\right)y^2 + \left(\frac{1}{n_e^2} + r_{33}E^{el}\right)z^2 = 1 \quad (2.37)$$

having no mixed terms in Eq 2.37 results in unchanged principle axis of modulated index ellipsoid. Lengths of axis in new index ellipsoid are in the form $n + \Delta n$ which is,

$$n_x = n_o - \frac{1}{2}n_o^3r_{13}E^{el} \quad (2.38a)$$

$$n_y = n_o - \frac{1}{2}n_o^3r_{13}E^{el} \quad (2.38b)$$

$$n_z = n_e - \frac{1}{2}n_e^3r_{33}E^{el} \quad (2.38c)$$

The terms containing E^{el} will be used to derive overlap integral in Section 2.7. If a light beam is propagating along x -direction then the refractive index it experiences is

$$n_z - n_y = (n_e - n_o) - \frac{1}{2}(n_e^3r_{33} - n_o^3r_{13})E^{el} \quad (2.39)$$

2.4 Optical Waveguide

Optical field is confined and propagates through this medium. During the propagation, optical field experiences modulated refractive index, that is to say, this is the medium where Pockles effect takes place. Early designs was consisting of titanium (Ti) diffused bulk LN waveguide. In this fabrication method, Ti-strip is diffused into host material bulk LN through thermal annealing and resulting medium satisfies weak guidance of optical wave in a relatively large optical mode area with respect to thin film (TF) applications. Large optical mode dictates also placement of microwave waveguides far away from optical modes, which is detrimental for overlap integral. Otherwise gold electrodes absorbs optical field based on plasmonic effects. As a result, having large mode area results in reduced overlap between RF and optical fields which leads to increase of $V_\pi.L$ values.

The ultimate aim is integrating EO modulators with a small footprint into CMOS electronic chips and this requires reduced drive voltages in optical waveguide sections [14] [15]. TFLNOI provides high optical field confinement so that RF and optical fields overlap and drive voltage decreases. This is one of the main reason to prefer thin-film-on-insulator structure other than bulky waveguides.

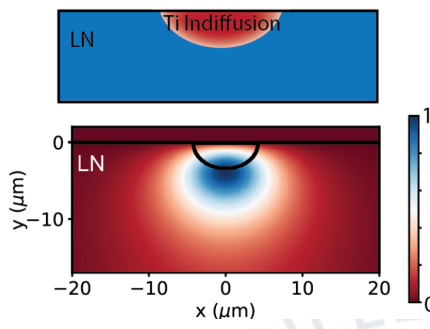


Figure 2.4: Overlap area in ion diffused LN waveguide is more than 10 times larger with respect to monolithic-rib-ridge waveguide on the right [1].

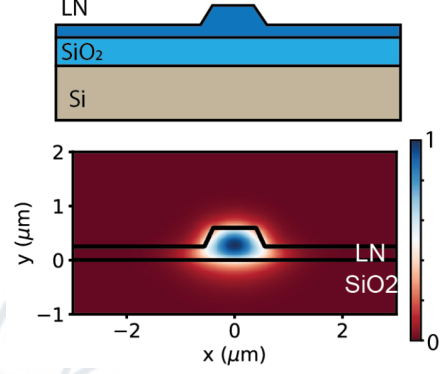


Figure 2.5: Monolithic-rib-ridge waveguide consists of oxide layer and a substrate in addition to LN [1].

In reference to crystal axis of LN, the direction in which bulk material is cut determines which polarization of E-field experiences extraordinary refractive index. Taking into account this condition, placement of electrodes supposed to be oriented in a way such that polarization of RF electric field and optical electric field matches with optical axis of the crystal.

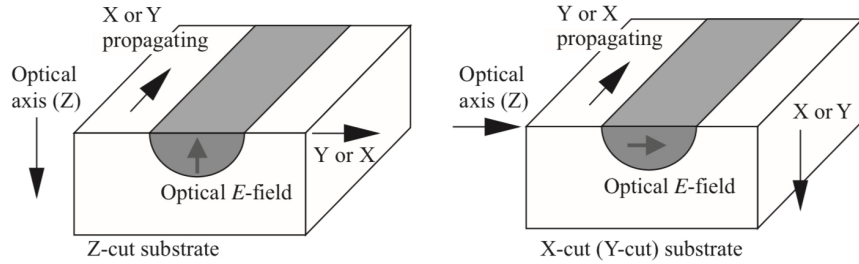


Figure 2.6: Cut direction in fabrication process determines modulator geometry [16] (the same directional reference applies also thin-film waveguides)

In figure 2.6 on the right, x-cut substrate is seen. In x-cut substrate, optical axis is in-plane of wafer surface. Optical field is through the optical axis of crystal. Corresponding mode polarization for optical electric field is TE-polarization. On the left, z-cut substrate is seen. This time optical field out-of-wafer-surface. This leads to dif-

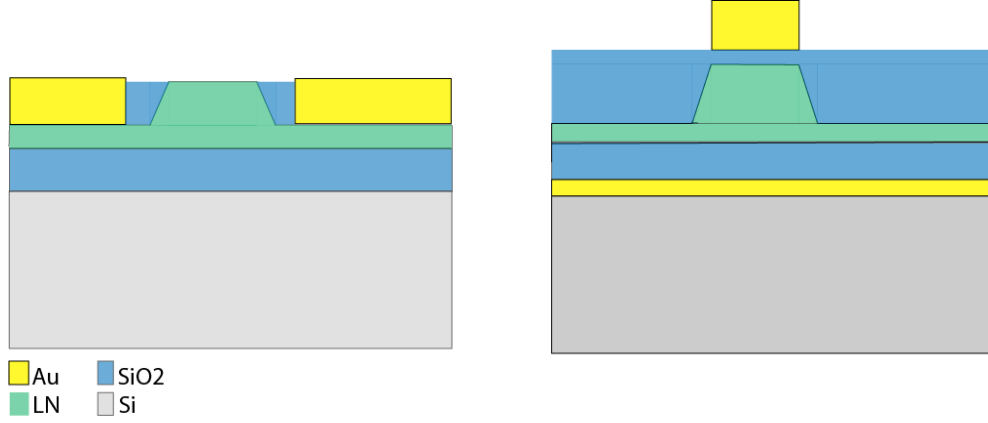


Figure 2.7: Electrodes are placed depending on crystal-cut so that overlap of fields achieved. X-cut LN is on the left and Z-cut LN is on the right

ferent electrode placement. In figure 2.7, microwave electrode placement is seen. On the left, electrodes are aligned horizontally in x-cut crystal structure and vertically aligned electrodes are seen on the right.

As for the application point of view, polarization maintaining fiber has to be utilized to ensure the polarization of the light shine onto integrated waveguide facet.

2.5 Coplanar Waveguide

Applied modulating field is in the range of GHz frequencies and this requires integration of microwave transmission line, or specifically coplanar waveguide. The wave has complex propagation constant,

$$\gamma_{el} = \alpha_{el} + j\beta_{el} = \alpha_{el} + j\frac{\omega}{c}n_{el} \quad (2.40)$$

where γ_{el} is complex microwave propagation constant, α_{el} [Np/m] is electrical losses and β_{el} [rad/m] is phase constant of the line and n_{el} microwave effective index.

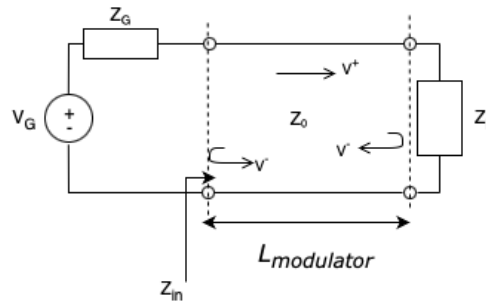


Figure 2.8: Generic microwave transmission line

In Figure 2.8, Z_0 corresponds to characteristic impedance of the line. It is considered as figure of merit for a transmission line and it is based on unit length parameters of the line, given in Figure 2.10. Characteristic impedance of lossy line is given as

$$Z_0 = \sqrt{\frac{R + j\omega L}{G + j\omega C}} \quad (2.41)$$

Another important parameter for microwave transmission line is input impedance as seen from the input of the line in figure

$$Z_{in} = Z_0 \frac{Z_L + Z_0 \tanh(\gamma_{el} l)}{Z_0 + Z_L \tanh(\gamma_{el} l)} \quad (2.42)$$

where Z_L is load impedance. Input impedance is depending on load, the electrical length and characteristic impedance of the transmission line .

The wave travelling through coplanar waveguide is in quasi-TEM mode, which assumes longitudinal field components is small relative to transverse field components. Several design parameters exist for coplanar waveguides such that,

1. Trace width (S)
2. Gap between signal and ground sections (w)
3. Effective dielectric constant of substrate (ϵ_{eff})
4. Thickness of dielectric (h)

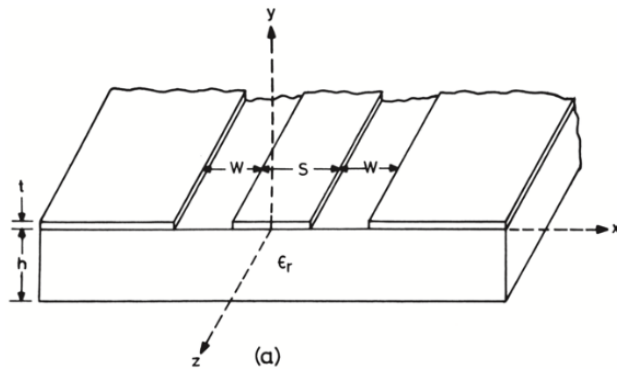


Figure 2.9: Geometry of coplanar waveguide [12]

As seen on Figure 2.7, multilayer structure consists of different materials which give rise to effective dielectric permittivity for microwave electric field, as opposed to Figure 2.9.

Lumped model of the line consists of equivalent resistance (R) and inductance of the line (L), line capacitance (C) and displacement field lossess (G) in dielectric.

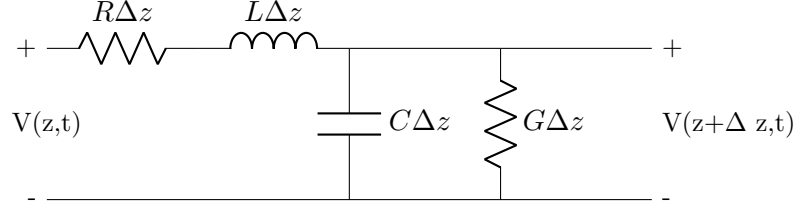


Figure 2.10: Unit length of coplanar waveguide

2.6 Mach Zehnder Electrooptic Modulator Types

Mach Zehnder modulators are based on interferometry phenomenon. In the context of this work, single electrode driving modulators are investigated. However, there are other types of driving applications which are called as dual electrode driving and two stage dual electrode driving in order to achieve more complex operations [20].

In the figure 2.11 basic phase modulator is seen on the left, it consists of microwave strip line and one optical waveguide. As for the one on the right, it is responsible from intensity modulation and it consists of CPW, MZI with 50:50 Y-splitter.

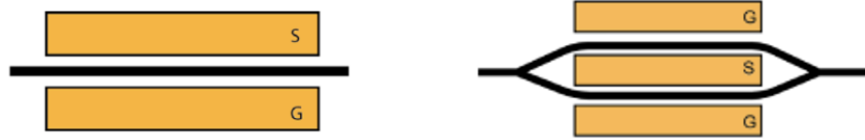


Figure 2.11: Phase modulator is seen on the left and MZI intensity modulator with upper and lower arms is on the right [1]

Phase modulator is basic building block of intensity modulation. In intensity modulation it is based on constructive and destructive interference. Excitation of V_π voltage causes 180° phase shift between two arms which ends up having destructive interference and "OFF" state. When there is no excitation applied, both arms are in phase which corresponds to "ON" state.

Static EO response starts with considering 3-port, matched, lossless Y-splitter with output ports are isolated. Following the notation in [16], scattering parameters of such structure is

$$\mathbf{S}_{sp} = \begin{bmatrix} 0 & \sqrt{\alpha} e^{j\phi_{sp}} & \sqrt{1-\alpha} e^{j\phi_{sp}} \\ \sqrt{\alpha} e^{j\phi_{sp}} & 0 & 0 \\ \sqrt{1-\alpha} e^{j\phi_{sp}} & 0 & 0 \end{bmatrix} \quad (2.43)$$

where α indicates power asymmetry for asymmetric splitter, for 50:50 splitter $\alpha = 0.5$. This matrix satisfies losslessness condition, $\mathbf{S}_{sp} \mathbf{S}_{sp}^\dagger = \mathbf{I}$. When its input power at port 1 is a_1 , output power at port 2 and port 3,

$$b_2 = \sqrt{\alpha} e^{j\phi_{sp}} a_1 \quad (2.44a)$$

$$b_3 = \sqrt{1-\alpha} e^{j\phi_{sp}} a_1 \quad (2.44b)$$

Scattering matrix for combiner, with input ports a'_2 (upper arm) and a'_3 (lower arm), is the same with splitter. The assumption for perfectly matched upper and lower arms is made and combiner inputs are

$$a'_2 = \sqrt{\alpha} e^{j\phi_{sp}} a_1 e^{-jk_0 L - j\Delta\phi_U} \quad (2.45a)$$

$$a'_3 = \sqrt{1-\alpha} e^{j\phi_{sp}} a_1 e^{-jk_0 L - j\Delta\phi_L} \quad (2.45b)$$

Then combiner output becomes

$$b'_1 = e^{2j\phi_{sp}} e^{-jk_0 L} \left[\alpha e^{-j\Delta\phi_U} + (1-\alpha) e^{-j\Delta\phi_L} \right] a_1 \quad (2.46)$$

Impedances are the same at the input and the output of the couplers, then

$$T(V_{in}) = \frac{P_{out}}{P_{in}} = \left| \frac{b'_1}{a_1} \right|^2 = \eta \{1 + 2\alpha(1-\alpha) [\cos(\Delta\phi_U - \Delta\phi_L) - 1]\} \quad (2.47)$$

where η represents optical insertion loss of the modulator. For the symmetrical case where $\alpha = 0.5$,

$$T(V_{in}) = \frac{\eta}{2} [1 + \cos(\Delta\phi_U - \Delta\phi_L)] \quad (2.48)$$

Splitters are symmetric but upper and lower arms may be asymmetrical. For this case, $V_{\pi U}$ and $V_{\pi L}$ are defined for $\Delta\phi_U = \pi$ and $\Delta\phi_L = -\pi$ as,

$$\Delta\phi_U = \pi \frac{v_{inU}}{V_{\pi U}} \quad (2.49a)$$

$$\Delta\phi_L = \pi \frac{v_{inL}}{V_{\pi L}} \quad (2.49b)$$

based on Eq 2.49, voltages $V_{\pi U,L}$ are calculated based on different overlap integral on the arms of MZI,

$$|\Delta\phi_{U,L}| = \frac{\pi n_e^3 r_{33} \Gamma_{\text{overlap}U,L}}{\lambda_0} \frac{L}{G} V_{\pi U,L} = \pi \rightarrow V_{\pi U,L} = \frac{G}{L} \frac{\lambda_0}{n_e^3 r_{33} \Gamma_{\text{overlap}U,L}} \quad (2.50)$$

Assuming that $v_{inU} = v_{inL} = v_{in}$, applying substitution Eq 2.50 back into 2.48,

$$T(V_{in}) = \frac{\eta}{2} \left\{ 1 + \cos \left[\pi \left(\frac{1}{V_{\pi U}} + \frac{1}{V_{\pi L}} \right) v_{in} \right] \right\} = \frac{\eta}{2} \left[1 + \cos \left(\pi \frac{v_{in}}{V_{\pi}} \right) \right] \quad (2.51)$$

where

$$V_{\pi} = \frac{V_{\pi U} V_{\pi L}}{V_{\pi U} + V_{\pi L}} \quad (2.52)$$

In Eq 2.51, the case where electrodes have different V_{π} voltages under the same excitation voltage is analyzed.

2.7 Electro-Optic Modulator Figure of Merits (FoM)

This section fundamentally contains the parameters help designer to define requirements of EOM. They can also indicate how efficient and high-speed the design is. For instance, efficiency is linked with half-wave voltage and high-speed is determined by bandwidth of the modulator. Insertion loss is also critical parameter affecting efficiency and extinction ratio measures how capable the modulator is to turn ON/OFF the output state.

2.7.1 Half-Wave Voltage (V_{π})

By itself half wave voltage (V_{π}) characterises power consumption. It corresponds to the voltage which is required to shift the phase of electric field by π radians in phase modulators. As for amplitude modulators, it is half of the voltage amplitude as in phase modulator, because of push-pull configuration. It is the most fundamental parameter and useful for both static and dynamic response.

Overlap integral is the term which relates externally applied modulating field to the modulated optical field. It is critical because microwave and optical fields are nonuniform over interaction region [16]. Derivation is based on perturbation of refractive index. In Eq 2.38, perturbation terms are simply denoted with $n + \Delta n$ and this also

causes perturbation in mode's propagation constant in Eq 2.10 as $\beta + \Delta\beta$. Due to Eq 2.10, is considered $(n + \Delta n)^2$ and approximated as $n^2 + 2n\Delta n$ and propagation constant is $(\beta + \Delta\beta)^2$ and is approximated as $\beta^2 + 2\beta\Delta\beta$. Substituting refractive index and propagation constant into Eq 2.10

$$\nabla_{\perp}^2 E^{op} + [(n^2 + 2n\Delta n)k_0^2 - (\beta^2 + 2\beta\Delta\beta)] E^{op} \approx [2n\Delta n k_0^2 - 2\beta\Delta\beta] E^{op} = 0 \quad (2.53)$$

Perturbed terms of both refractive index and propagation constant are under consideration, this is the reason of approximation in Eq 2.53. Then multiplying both sides with complex conjugate of optical electric field, $(E^{op})^*$, and integrating over waveguide cross-section

$$\int \int |E^{op}(x, y)|^2 n_e \Delta n_e dS = n_{TE} \Delta n_{TE} \int \int |E^{op}(x, y)|^2 dS \quad (2.54)$$

where $n \approx n_e$ and since $\beta_{TE} = n_{TE}k_0$ and n_{TE} is effective refractive index of the optical mode confined in LN area. Then,

$$\Delta n_{TE} = \frac{1}{n_{TE}} \frac{\int \int |E^{op}(x, y)|^2 n_e \Delta n_e dS}{\int \int |E^{op}(x, y)|^2 dS} \quad (2.55)$$

substituting perturbation in Eq 2.38c into above equation,

$$\Delta n_{TE} = -\frac{n_e^4 r_{33}}{2n_{TE}} \frac{\int \int |E^{op}(x, y)|^2 E^{el}(x, y) dS}{\int \int |E^{op}(x, y)|^2 dS} \quad (2.56)$$

by normalizing $E^{el}(x, y)$ with respect to uniform field induced by voltage V over distance G

$$e_z(x, y) = \frac{G}{V} E^{el}(x, y)$$

and perturbation in refractive index is written in terms of overlap integral as,

$$\Delta n_{TE} = -\frac{n_e^4 r_{33} V}{2n_{TE} G} \Gamma_{overlap} \quad (2.57)$$

where $\Gamma_{overlap}$ is written as,

$$\Gamma_{overlap} = \frac{G}{V} \frac{\int \int |E^{op}(x, y)|^2 E^{el}(x, y) dS}{\int \int |E^{op}(x, y)|^2 dS} \quad (2.58)$$

In case of MZM, G represents the gap between the microwave electrodes and V is applied voltage amplitude of microwave field.

Phase shift introduced by modulated refractive index is seen as

$$\Delta\phi = \frac{2\pi\Delta n_{TE}}{\lambda_0}L \quad (2.59)$$

where L indicates interaction length or modulator length. Keeping in mind the symmetric case where $\Delta\phi_{upper} = -\Delta\phi_{lower}$ When phase difference is $\frac{\pi}{2}$, output power of modulator goes to minimum.

$$\frac{\pi}{2} = \frac{2\pi}{\lambda_0} \frac{n_e^4 r_{33} V}{2n_{TE} G} \Gamma_{overlap} L \quad (2.60)$$

Then V_π voltage becomes

$$V_\pi = \frac{\lambda_0 n_{TE}}{2n_e^4 r_{33} \Gamma_{overlap}} \frac{G}{L} \quad (2.61)$$

$V_\pi . L$ multiplication is pronounced in phase modulators since it indicates the phase shift introduced through modulator length L .

2.7.2 Modulation Bandwidth

Modulation bandwidth is considered as frequency dependent characteristic of modulator and this means it is related with dynamic response. Most common bandwidth definitions are 3dB and 6dB bandwidth, where modulation efficiency drops by 3 dB and 6 dB from the reference frequency [1]. The reference frequency can be chosen as DC or higher frequency such as 1GHz.

Analysis of bandwidth requires investigation of microwave electric field, which is generated by voltage wave on the waveguide. Following the notation given in [16], general solution of voltage wave equation on a transmission line is

$$\tilde{V}(z) = V^+(z) + V^-(z) = V_o^+ e^{-\gamma_{el} z} + V_o^- e^{\gamma_{el} z} \quad (2.62)$$

where \tilde{V} and \tilde{I} indicates voltage and current phasors, respectively and $V_o^+(z)$ is forward propagating incident voltage wave, $V_o^-(z)$ is backward propagating reflected voltage wave. Transition from frequency domain to time domain is achieved by $v(z, t) = \Re\{\tilde{V}(z)e^{j\omega t}\}$. Time domain waveforms has easiness in analysis of wave velocities. The interaction between optical and electrical waves and its effect on bandwidth is discussed through their wave velocities.

$$V(z, t) = V_o^+ e^{j\omega(t - \frac{z}{v_{el}}) - \gamma_{el}z} + V_o^- e^{j\omega(t + \frac{z}{v_{el}}) + \gamma_{el}z} \quad (2.63)$$

The relationship between refractive index change and time-changing voltage relation can be represented with Eq (2.57) by small modification of time and position dependence

$$\Delta n_{TE}(z, t) = aV(z, t) \quad (2.64)$$

Change of optical mode's phase is obtained by integrating the refractive index change through modulator length L , based on Eq (2.59),

$$\Delta\phi = k_0 \int_0^L \Delta n(z, t_2 - \frac{L}{v_o} + \frac{z}{v_o}) dz \quad (2.65)$$

where t_2 corresponds to the time when optical mode reaches the end of modulator and time t defined as $t = t_2 - \frac{L}{v_o} + \frac{z}{v_o}$ to emphasize the relation between optical group velocity and microwave phase velocity. By considering Eq (2.63), (2.64), (2.65), optical phase change is calculated as,

$$\Delta\phi = k_0 a e^{j\omega(t_2 - \frac{L}{v_o})} \left[\frac{V^+ e^{j\omega(\frac{L}{v_o} - \frac{L}{v_m}) - \alpha_m L} - 1}{j\omega(\frac{1}{v_o} - \frac{1}{v_m}) - \alpha_m} + \frac{V^- e^{j\omega(\frac{L}{v_o} + \frac{L}{v_m}) + \alpha_m L} - 1}{j\omega(\frac{1}{v_o} + \frac{1}{v_m}) + \alpha_m} \right] \quad (2.66)$$

Critical thing here is that there are three assumptions which leads to design of high speed electro-optic modulator design. Firstly, if characteristic impedance matching is achieved with load and generator impedances there will be no backward travelling V^- term to deteriorate phase change. Then, if optical group velocity and microwave phase velocities are matched there will be no phase term and imaginary term in V^+ term in nominator and denominator, respectively. These two are necessary to design proper TFLN electro-optical modulator design. After achieving these matching, equation becomes,

$$\Delta\phi = k_0 a e^{j\omega(t_2 - \frac{L}{v_o})} \left[V^+ \frac{e^{-\alpha_m L} - 1}{-\alpha_m} \right] \quad (2.67)$$

This last equation can be interpreted as the design of cutting-edge TFLN EO modulator should have small microwave losses for a large bandwidth or improved dispersion characteristics.

As a result, modulation bandwidth is based on three critical parameters which are velocity matching, impedance matching and microwave losses.

Velocity Matching

In order to achieve stable modulation, velocity of optical signal and microwave signal are supposed to match. Modulation fundamentally generates sidebands and this leads to new frequency components in optical signal. Due to this fact, group velocity of optical signal is matched to the phase velocity of microwave field so that phase fronts of microwave coincide with "wave packets" of optical signal. By definitions, centroid of optical fields travel at the group velocity of

$$v_g^{opt} = \frac{d\omega^{opt}}{d\beta^{opt}} \quad (2.68)$$

where ω^{opt} angular frequency of optical signal and β^{opt} propagation constant of optical signal.

Considering energy and momentum conservation in the concept of modulation, change of optical frequency, $\Delta\omega^{opt}$, is supposed to be equal to microwave frequency ω^{el} . Moreover, momentum conservation dictates $\Delta\beta^{opt} = \beta^{el}$

Impedance Matching

Impedance matching is critical for efficient power transfer in microwave transmission lines. In general, mismatch is caused by any difference from characteristic impedance of the transmission line. Mismatch is demonstrated mathematically S_{11} parameter, belonging to $S - matrix$, of two port microwave network.

$$S_{11} = \Gamma_{reflection} = \frac{Z_L - Z_0}{Z_L + Z_0} \quad (2.69)$$

The reflected wave will generate a standing wave together with incident wave travelling through coplanar waveguide. This standing wave causes degradation in frequency response of EOM.

Microwave Losses

Small gap distance around $5 \mu m$ causes high microwave field confinement and accumulation of current at the edges of metallic coplanar waveguide. Typical loss levels for this geometry around $1 dB cm^{-1}$ [1], as seen in figure 2.8. In order to prevent accumulation

of current at the edges through gap, metallic waveguide is microstructured as small segments and new loss level for manufactured geometry reduces approximately to 0.26 dB cm⁻¹ [19].

Calculation of particular solutions of propagating voltage waves, V^+ and V^- , in Eq (2.65, is done by applying boundary conditions of at the beginning and at the load-end of transmission line. Eventually modulation index is obtained such that

$$m(\omega) = \left| \frac{2Z_{in}}{Z_{in} + Z_L} \right| \left| \frac{(Z_L + Z_0)F_+ + (Z_L - Z_0)F_-}{(Z_L + Z_0)e^{\gamma_{el}L} + (Z_L - Z_0)e^{-\gamma_{el}L}} \right| \quad (2.70)$$

where $F(u) = \frac{1-e^u}{u}$ and $u_{\pm}(\omega) = j(\beta_{el} - \beta_o)L \pm \gamma_{el}L = \pm\gamma_{el}L + j\frac{\omega}{c_o}(\pm n_{el} - n_o)$ accounts for forward and backward propagating waves, Z_L is load impedance, Z_{in} is input impedance as seen at the input of CPW, Z_{in} is characteristic impedance of the CPW.

2.7.3 Insertion Loss

Insertion loss causes degradation in power of guided optical wave and it is caused by fiber-to-chip coupling and on chip insertion loss [1]. This project focuses on-chip insertion loss and specifically metallic absorption in electrodes, and other reasons of on chip loss are wave propagation and bending loss and insertion loss of splitters/combiners. Typical loss levels for wave propagation in LN is seen in Table 1.2.

2.7.4 Extinction Ratio

Extinction ratio one of the critical parameters determining on-off state output power ratio for intensity modulators. Possible mismatches between arms of MZM cause degradation of output power. Mismatches may include unbalanced loss between arms and splitter/combiner imperfections. Typical value for an extinction ratio is 30dB [14].

3. METHODS AND RESULTS

This section consists of the simulation physics which are utilized and simulation results of X-cut Z-cut EO modulators.

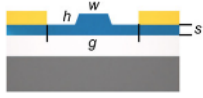
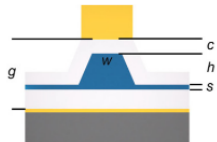
There are two simulation physics utilized one of them is to determine optical field mode in TFLN waveguide and it is called as *Electromagnetics Wave, Frequency Domain (ewfd)*. The other physic utilized is *Electrostatics (es)* to simulate static field distribution through gap area of CPW.

Firstly, simulation configurations are checked by realizing the geometry based on the paper [21]. The mode confinement and overlap with DC field distribution are derived from COMSOL 6.0. Then COMSOL-MATLAB Livelink is utilized in order to calculate overlap integral and V_π voltage is calculated based on that value. After than that, another simulation was run for the modulator which Girish Karthik experimentally measured in the laboratory and results are compared. Finally, parametric simulations are done to observe how $V_\pi L$ value responds to these changes and to see how loss can be limiting factor to realize some of the modulator geometries.

Verification of Simulation

Zhang et al. [21] has calculated V_π voltages for different thin film optical waveguides.

Table 3.1: X-cut and Z-cut TFLN modulator dimensions and calculated $V_\pi \cdot L$ values by Zhang et al. [21]

Label	X-Cut LN	Z-Cut LN
Structure		
Slab thickness (s)	200 nm	300 nm
Ridge height (h)	400 nm	1.2 μm
Ridge width (w)	770 nm	800 nm
Cladding thickness (c)	Parametric	3.2 μm
Metal gap (g)	2 μm	700 nm
$V_\pi \cdot L$ (push-pull)	2.25 V.cm	2.6 V.cm

In their study, they focused on all-LN x-cut rib waveguide desing and all-LN z-cut

rib waveguide design with planar electrode, which is in line with the aim of this work.

In the table 3.1, calculated $V_\pi \cdot L$ values and corresponding dimensions are given. In this work, $V_\pi L$ product is calculated to verify the simulation physics used and parameter configurations.

Geometry	Mode Index	Overlap	$V_\pi L$
X-cut	1.8872	0.5230	2.1679V
Z-cut	2.029	0.3516	2.4117V

Table 3.2: Simulation results for X-cut and Z-cut Modulators

In table 3.2, the results of simulations, are done in this work, are seen. Mode index difference occurs due to different ridge height in two waveguide. As the ridge height decreases, wave will be more confined and the difference between mode index and material's refractive index increases. Also, large overlap value is result of having confinement in small region.

Table 3.3: $V_\pi L$ voltage comparison of this work with the ones obtained by Zhang et al. [21]

X-Cut Modulator		Z-cut Modulator	
This Work	Paper	This Work	Paper
2.1679 V.cm	2.25 V.cm	2.4117 V.cm	2.60 V.cm

Zhang et al. [21] has indicated that $V_\pi \cdot L$ values in their paper are quantitative results for starting design of abovementioned geometries. This means values are not optimized. In the light of this information, percent error is calculated as 3.65% in X-cut modulator and 7.24% in Z-cut modulator.

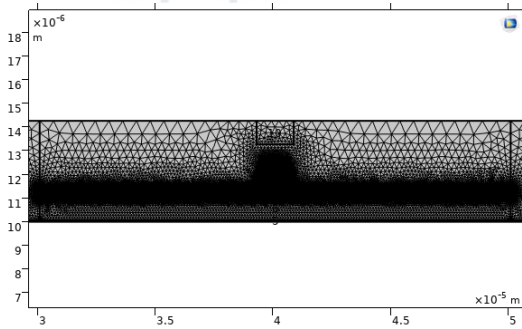


Figure 3.1: Optical mesh which COMSOL *EM Wave Frequency Domain (ewfd)* generates

In Figure 3.1 and 3.2 measured meshes are seen. In order to precisely solve the domains where field modes confine, polygon definition is made and the region inside

that polygon has more precise mesh.

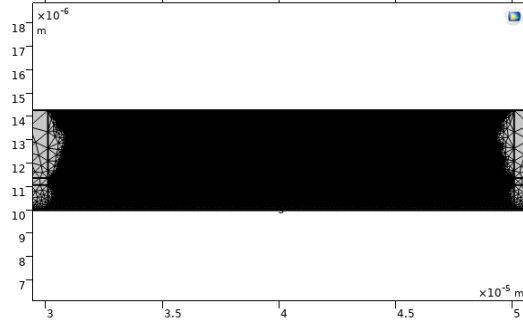


Figure 3.2: DC mesh which COMSOL *Electrostatic (es)* generates

Experimentally Verified V_π

Transmission characteristic of sample EO MZM is seen in Figure 3.3 and measurement process was carried out by Girish Karthik.

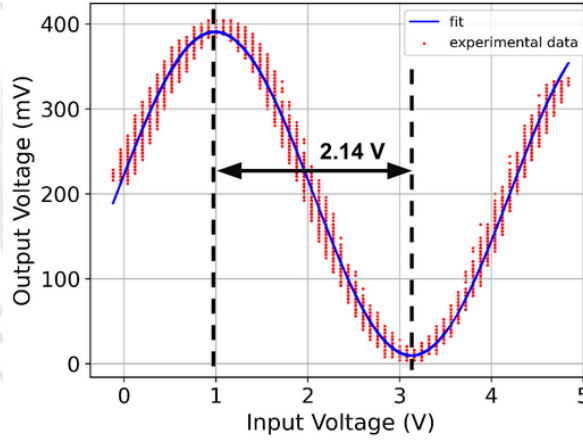


Figure 3.3: Transmission characteristic of sample modulator with length of 0.920cm. Red dots represents experimental data which is sampled by oscilloscope.

Since $V_\pi L$ voltage is constant and voltage and length of modulator is inversely proportional, 1-cm-modulator has smaller voltage value which is seen in Table 3.4. Percent error between experimental and simulation data is 29.7%.

Method	Mode Index	Overlap	$V_\pi L$
Realized Measurement	-	-	1.969 V.cm
Simulation	1.9125	0.2598	2.8301 V.cm

Table 3.4: Experimentally measured $V_\pi L$ value and its simulation results

Parametric Sweep In X-cut Modulator - $V_\pi L$ And Top SiO_2 Layer Dependence

Thickness change of top layer silica has effect on the overlap integral. As the microwave electrodes moves away from optical waveguide, overlap integral decreases. This effect can be seen on the figure 3.4.

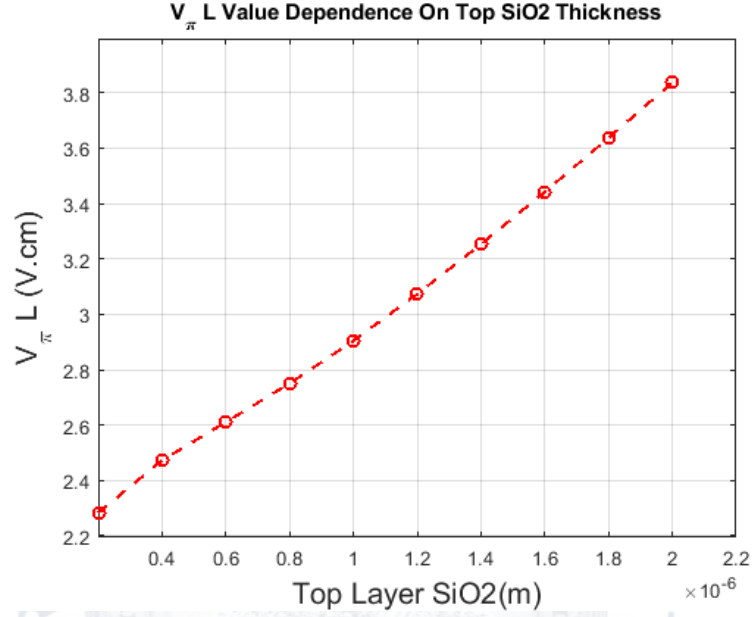


Figure 3.4: In x-cut EO MZM, top layer silica has changed and reduced

In order to have small V_π value, one can think to place the electrodes as close as possible to optical waveguide. However, plasmonic behavior start to arise in that case since metal-dielectric boundary becomes easily available for the optical wave and optical confinement is not achieved. This effect is seen in figure 3.5.

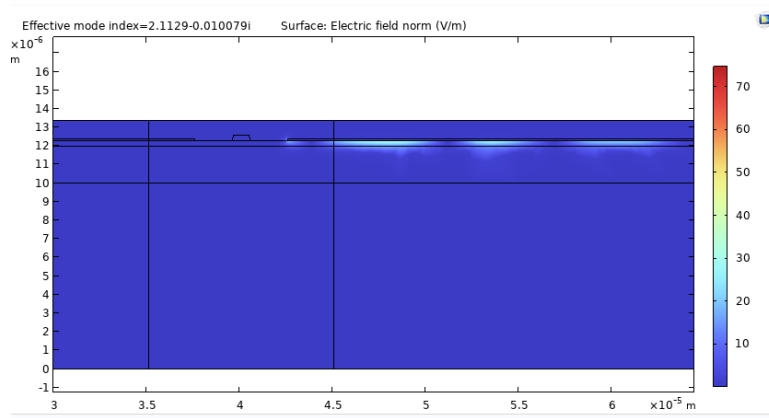


Figure 3.5: Plasmonic behavior in metal-LN interface. Silica layer is removed in this case.

The top silica layer helps preserve optical confinement and the overlap integral, preventing degradation that would otherwise increase optical loss

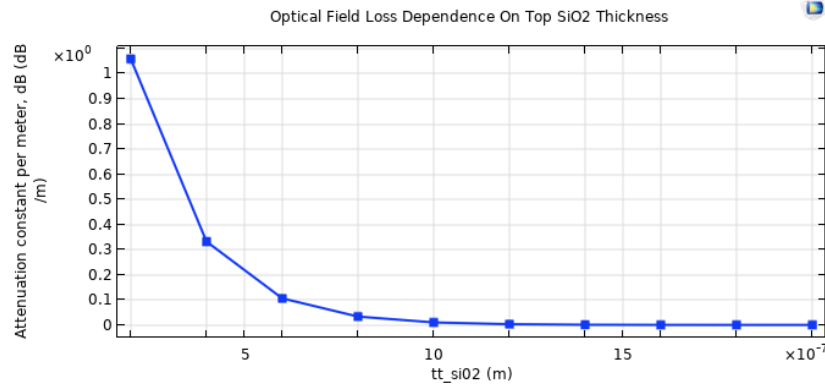


Figure 3.6: In x-cut EO MZM, top layer silica (x-axis) has parametrically changed and corresponding loss values are observed.

As it is seen on figure 3.6, if the metallic electrodes are close to optical waveguide losses (dB/m) will increase. Critical observation would be the speed of change, it can be represented in linear scale, instead of logarithmic one. However, it is still undesirable.

Parametric Sweep In X-cut Modulator - $V_{\pi}L$ And Coplanar Waveguide Gap Dependence

Another approach to increase overlap between optical and microwave fields is having smaller gap between coplanar waveguide signal and ground electrodes.

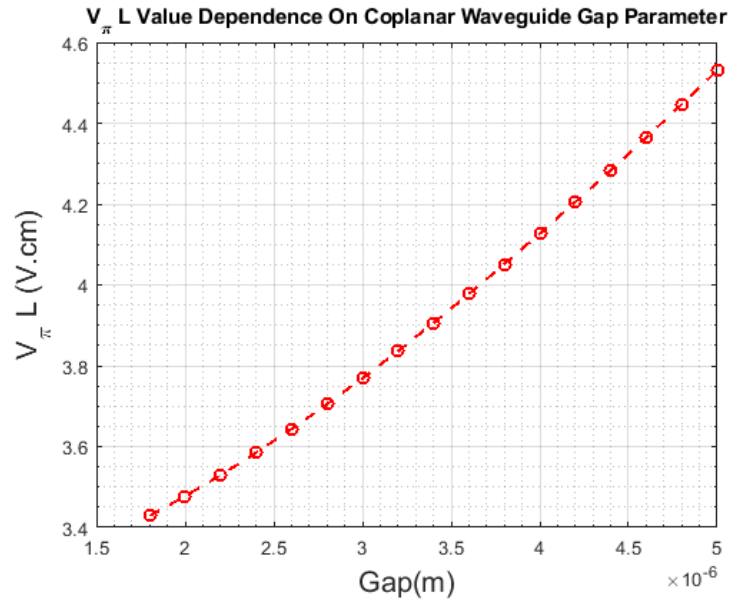


Figure 3.7: In x-cut EO MZM, gap between microwave electrodes has parametrically swept.

$V_\pi L$ value change almost linearly with respect to gap parameter in figure 3.7. Also, plasmonic effects still persist. This requires loss analysis for optical mode. In figure 3.8, change of loss in response to gap change is fast and small in amplitude. Increasing distance may decrease loss however it degrades V_π voltage.

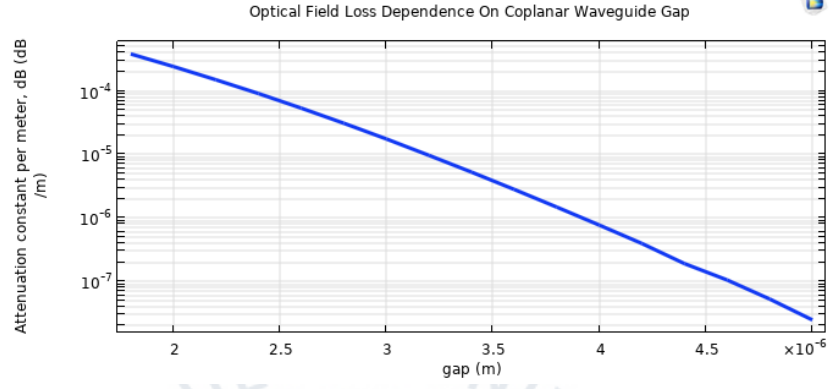


Figure 3.8: In x-cut EO MZM, change of gap and its effect on optical loss is seen. Vertical scale is logarithmic.

Parametric Sweep In Z-cut Modulator - $V_\pi L$ And Top SiO_2 Layer Dependence

Z-cut modulators have different microwave electrode orientation due to the reason mentioned in Optical Waveguides section. In this configuration top silica layer thickness has crucial effect on overlap integral and overall performance of the device.

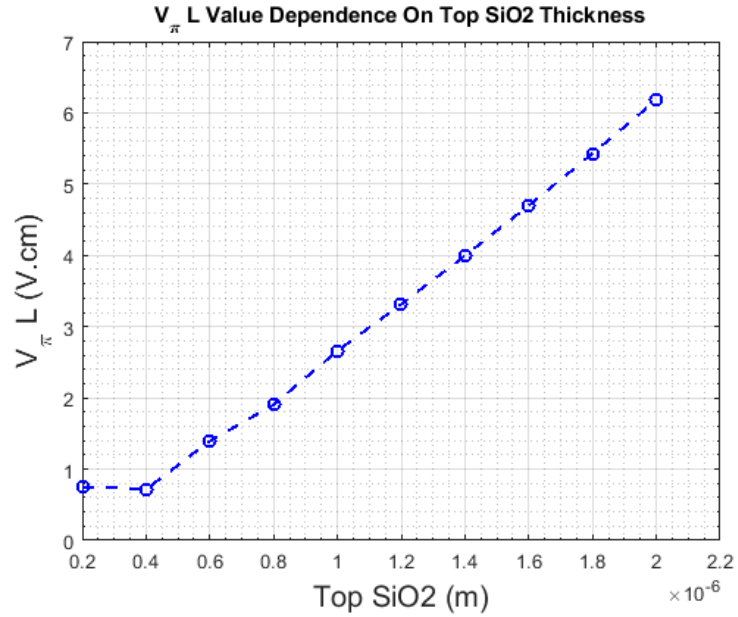


Figure 3.9: In z-cut EO MZM, change of top silica layer and $V_\pi L$ value relation is seen.

For a proper comparison, x-cut and z-cut modulators have both same top silica sweeps. However, z-cut modulator does not works properly for 200nm and 400nm top silica thicknesses because electrode overlaps with optical waveguide, which leads to unrealizable geometry. This result is seen in figure 3.9. Considering $V_{\pi}L$ values starting from 600nm, they are almost linearly dependent on top silica thickness.

As for optical loss in z-cut modulator, it is drastically affected from top silica thickness. In figure 3.10, vertical scale indicates loss (dB/m) and it is represented in logarithmic scale.

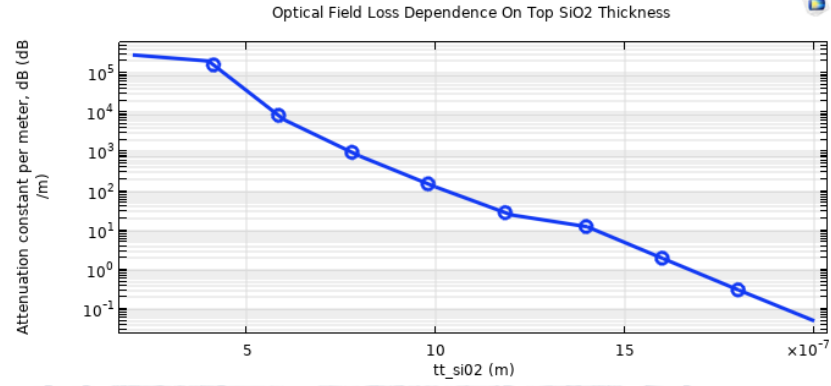


Figure 3.10: In z-cut EO MZM, change of top silica layer has strong impact on optical loss

For this large loss value, optical field does not confine in nonlinear medium, as in figure 3.11 and overlap integral degrades. Moreover, this unconfined mode supports the profitless $V_{\pi}L$ voltages for 200nm and 400nm in figure 3.9.

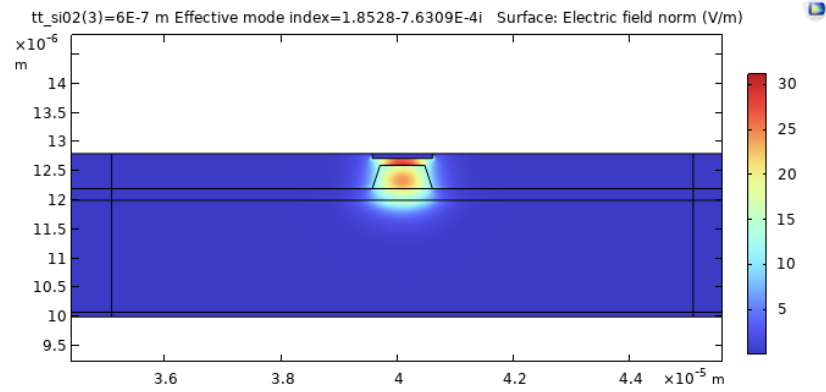


Figure 3.11: Due to severe loss, optical mode does not confine in z-cut modulator

4. DISCUSSION

Abovementioned simulation results demonstrate the two different EO MZM geometries, x-cut and z-cut, by highlighting difference in overlap integral and V_π voltage.

Firstly, simulation methodology is compared by analysing already-studied-parameters in [21]. Zhang et al. have studied x-cut and z-cut modulators in a more quantitative way as it is mentioned in their paper. Due to this reason, percent error around 3% to 7% is understandable. As for experimental $V_\pi L$ measurement, simulations still provide general idea about expected $V_\pi L$ value, however, it may not be possible to pinpoint exact experimental value using simulations because the computational power and the time spent on modelling several physics and integrating them in multi-physics simulation environment can not be underestimated. Moreover, data collection process in experimental measurement for example oscilloscope's data sampling method should be discussed.

Secondly, parametric sweeps are introduced in order to show how $V_\pi L$ value changes based on the change in distance between electrodes. The most drastic change occurred in Z-cut modulator's top silica layer thickness simulations. Here, optical mode is mostly absorbed by Au-electrodes. This result supports why x-cut modulators are preferred over z-cut modulators.

In figure 4.1, even if z-cut modulator has smaller $V_\pi L$ value for smaller top silica thickness, it is not applicable to realize that lossy design. Also, x-cut is more versatile due to its electrode structure. CPW's are easy to manufacture and to adjust and has extensive study [12].

Requiring less $V_\pi L$ value in design means having more power-efficient modulator. Since x-cut modulators have less V_π voltage and more efficient with respect to z-cut modulators, it is easier to integrate them in CMOS applications with control voltages less than or equal to 5V.

Finally, x-cut modulators are more efficient and this efficiency makes them suitable for more applications.

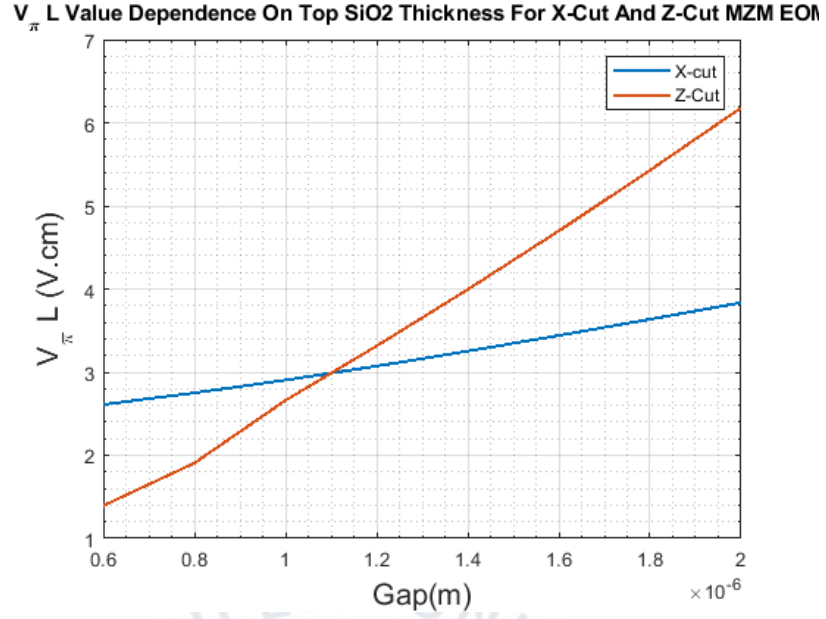


Figure 4.1: $V_{\pi}L$ values are compared for different modulators.

4.0.1 Future Work

Particularly for this work, V_{π} precision may be increased by also introducing frequency dependent microwave simulations so that bandwidth is also analyzed. Experimentally measured $V_{\pi}L$ value can be compared with dynamic response simulation results so that the experimental data which suffers from unstable DC reference frequency is omitted and higher reference frequency is preferred. Then percent error can be reduced. Moreover, this brings more realistic behavior since different loss mechanisms will be introduced. Eventually, there will be more analysis on losses by introducing new physics.

Bibliography

- [1] Di Zhu, Linbo Shao, Mengjie Yu, Rebecca Cheng, Boris Desiatov, C. J. Xin, Yaowen Hu, Jeffrey Holzgrafe, Soumya Ghosh, Amirhassan Shams-Ansari, Eric Puma, Neil Sinclair, Christian Reimer, Mian Zhang, and Marko Lončar, "Integrated photonics on thin-film lithium niobate," *Adv. Opt. Photon.* 13, 242-352 (2021)
- [2] Yariv, Amnon, and Pochi Yeh. 2007. *Photonics: Optical Electronics in Modern Communications* (version Public Access - front matter, author index, subject index). Oxford, UK: Oxford University Press.
- [3] Ling Liao, Dean Samara-Rubio, Michael Morse, Ansheng Liu, Dexter Hodge, Doron Rubin, Ulrich D. Keil, and Thorkild Franck, "High speed silicon Mach-Zehnder modulator," *Opt. Express* 13, 3129-3135 (2005)
- [4] M. Qasymeh, M. Cada and S. A. Ponomarenko, "Quadratic Electro-Optic Kerr Effect: Applications to Photonic Devices," in *IEEE Journal of Quantum Electronics*, vol. 44, no. 8, pp. 740-746, Aug. 2008, doi: 10.1109/JQE.2008.924430.
- [5] W. -T. Huang et al., "Emerging Modulator Technologies in Silicon Photonics," in *IEEE Nanotechnology Magazine*, doi: 10.1109/MNANO.2025.3551177.
- [6] B. Jalali and S. Fathpour, "Silicon Photonics," in *Journal of Lightwave Technology*, vol. 24, no. 12, pp. 4600-4615, Dec. 2006, doi: 10.1109/JLT.2006.885782.
- [7] Smit, Meint, Kevin Williams, and Jos Van Der Tol. "Past, present, and future of InP-based photonic integration." *Apl Photonics* 4.5 (2019).
- [8] N. Courjal et al., 'Lithium Niobate Optical Waveguides and Microwaveguides', *Emerging Waveguide Technology*. InTech, Aug. 01, 2018. doi: 10.5772/intechopen.76798.
- [9] Terrasanta, Giulio, et al. "Photonic Integrated Circuits for Optical Satellite Links: A Review of the Technology Status and Space Effects." *International Journal of Satellite Communications and Networking* (2025).

- [10] Robert W. Boyd, "Nonlinear Optics", 4th Edition, 2020, Academic Press, ISBN: 978-0-12-811002-7
- [11] Frits Zernike, John E. Midwinter, "Applied Nonlinear Optics", 1973 Dover Publications, New York.
- [12] Inder Bahl, Maurizio Bozzi, Ramesh Garg, "Microstrip Lines and Slotlines", Third Edition, Artech, 2013.
- [13] Yanting Guo, Lianyan Li, Yunshan Zhang, Shiyuan Sun, Qihong Quan, and Yuechun Shi, "Equivalent circuit model of the traveling wave electrode for lithium niobate thin film Mach–Zehnder modulators," *Appl. Opt.* 63, 617-623 (2024)
- [14] Wang, C., Zhang, M., Chen, X. et al. Integrated lithium niobate electro-optic modulators operating at CMOS-compatible voltages. *Nature* 562, 101–104 (2018)
- [15] Cheng Wang, Mian Zhang, Brian Stern, Michal Lipson, and Marko Lončar, "Nanophotonic lithium niobate electro-optic modulators," *Opt. Express* 26, 1547-1555 (2018)
- [16] Ghione G. *Semiconductor Devices for High-Speed Optoelectronics*. Cambridge University Press; 2009.
- [17] J. P. Salvestrini, L. Guilbert, M. Fontana, M. Abarkan and S. Gille, "Analysis and Control of the DC Drift in LiNbO₃Based Mach–Zehnder Modulators," in *Journal of Lightwave Technology*, vol. 29, no. 10, pp. 1522-1534, May15, 2011.
- [18] Shihao Sun, Mingbo He, Mengyue Xu, Shengqian Gao, Ziyang Chen, Xian Zhang, Ziliang Ruan, Xiong Wu, Lidan Zhou, Lin Liu, Chao Lu, Changjian Guo, Liu Liu, Siyuan Yu, and Xinlun Cai, "Bias-drift-free Mach–Zehnder modulators based on a heterogeneous silicon and lithium niobate platform," *Photon. Res.* 8, 1958-1963, 2020.
- [19] Prashanta Kharel, Christian Reimer, Kevin Luke, Lingyan He, and Mian Zhang, "Breaking voltage–bandwidth limits in integrated lithium niobate modulators using micro-structured electrodes," *Optica* 8, 357-363 (2021).
- [20] Q. He, J. Wang, C. Zeng, G. He and X. Xu, "Analysis and Design of High-Accuracy Driving Circuit for Wideband Phase Modulators," in *IEEE Instrumentation & Measurement Magazine*, vol. 27, no. 4, pp. 76-82, June 2024.

- [21] Mian Zhang, Cheng Wang, Prashanta Kharel, Di Zhu, and Marko Lončar, "Integrated lithium niobate electro-optic modulators: when performance meets scalability," *Optica* 8, 652-667 (2021)

